

Modeling of high permittivity insulator structure with interface charge by charge compensation

Zhi-Gang Wang(汪志刚) , Yun-Feng Gong(龚云峰), and Zhuang Liu(刘壮)

Citation: Chin. Phys. B, 2022, 31 (**2**): 028501. DOI: 10.1088/1674-1056/ac0cd3
Journal homepage: http://cpb.iphy.ac.cn; http://iopscience.iop.org/cpb

What follows is a list of articles you may be interested in

A 3D SiC MOSFET with poly-silicon/SiC heterojunction diode

Sheng-Long Ran(冉胜龙), Zhi-Yong Huang(黄智勇), Sheng-Dong Hu(胡盛东), Han Yang(杨晗), Jie Jiang(江洁), and Du Zhou(周读)

Chin. Phys. B, 2022, 31 (**1**): 018504. DOI: 10.1088/1674-1056/ac0038

Trigger mechanism of PDSOI NMOS devices for ESD protection operating under elevated temperatures

Jia-Xin Wang(王加鑫), Xiao-Jing Li(李晓静), Fa-Zhan Zhao(赵发展), Chuan-Bin Zeng(曾传滨), Duo-Li Li(李多力), Lin-Chun Gao(高林春), Jiang-Jiang Li(李江江), Bo Li(李博), Zheng-Sheng Han(韩郑生), and Jia-Jun Luo(罗家俊)

Chin. Phys. B, 2021, 30 (**7**): 078501. DOI: 10.1088/1674-1056/abe2fe

Improved 4H-SiC UMOSFET with super-junction shield region

Pei Shen(沈培), Ying Wang(王颖), Xing-Ji Li(李兴冀), Jian-Qun Yang(杨剑群), Cheng-Hao Yu(于成浩), and Fei Cao(曹菲)

Chin. Phys. B, 2021, 30 (**5**): 058502. DOI: 10.1088/1674-1056/abd740

Novel Si/SiC heterojunction lateral double-diffused metal-oxide semiconductor field-effect transistor with p-type buried layer breaking silicon limit

Baoxing Duan(段宝兴), Xin Huang(黄鑫), Haitao Song (宋海涛), Yandong Wang(王彦东), and Yintang Yang(杨银堂)

Chin. Phys. B, 2021, 30 (**4**): 048503. DOI: 10.1088/1674-1056/abcf45

Total dose test with *γ*-ray for silicon single photon avalanche diodes

Qiaoli Liu(刘巧莉), Haiyan Zhang(张海燕), Lingxiang Hao(郝凌翔), Anqi Hu(胡安琪), Guang Wu(吴光), Xia Guo(郭霞)

Chin. Phys. B, 2020, 29 (**8**): 088501. DOI: 10.1088/1674-1056/ab9286

Modeling of high permittivity insulator structure with interface charge by charge compensation

Zhi-Gang Wang(汪志刚)†, Yun-Feng Gong(龚云峰), and Zhuang Liu(刘壮)

School of Information Science and Technology, Southwest Jiao Tong University, Chengdu 611756, *China*

(Received 23 April 2021; revised manuscript received 15 June 2021; accepted manuscript online 21 June 2021)

An analytical model of the power metal–oxide–semiconductor field-effect transistor (MOSFET) with high permittivity insulator structure (HKMOS) with interface charge is established based on superposition and developed for optimization by charge compensation. In light of charge compensation, the disturbance aroused by interface charge is efficiently compromised by introducing extra charge for maximizing breakdown voltage (BV) and minimizing specific ON-resistance ($R_{on,sp}$). From this optimization method, it is very efficient to obtain the design parameters to overcome the difficulty in implementing the $R_{on,sp}$–BV trade-off for quick design. The analytical results prove that in the HKMOS with positive or negative interface charge at a given length of drift region, the extraction of the parameters is qualitatively and quantitatively optimized for trading off BV and $R_{on,sp}$ with JFET effect taken into account.

Keywords: charge compensation, breakdown voltage, high permittivity, interface charge, super-junction

PACS: 85.30.De, 51.50.+v **DOI:** 10.1088/1674-1056/ac0cd3

1. Introduction

Today, the power metal–oxide–semiconductor field-effect transistor (MOSFET) with high permittivity insulator structure (HKMOS) as a prospective power semiconductor switching has excellent advantages for applications in the low and medium power field.[1–4] The high permittivity (HK) pillar introduced into power MOSFET has no problem of charge imbalance potentially and replaces the superjunction (SJ), thereby optimizing the trade-off between specific ON-resistance ($R_{on,sp}$) and breakdown voltage (BV) of power MOSFETs.[5,6] However, the existence of interface charge at the hetero-interface between HK pillar and silicon pillar is unavoidable, resulting in pre-avalanche breakdown.[7–9] Therefore, the quick designing of BV and $R_{on,sp}$, which is dependent not only on drift region doping concentration, but also on interface charge, becomes a complex work to facilitate the optimization.[10–13] Owing to material-dependent HK pillar, $BV^2/R_{on,sp}$ regarded as the figure of merit gives a useful insight into the assessment of compromising BV–$R_{on,sp}$.[14,15] Although BV varies in a range of −8.1%–5.3% with unintentional penalty in $R_{on,sp}$ increment affected by HK pillar,[16,17] in the case of HKMOS with interface charge, the BV–$R_{on,sp}$ trade-off becomes difficult to account for.

In this paper, the HKMOS with interface charge evolves into the HKMOS with charge-compensation region (C^{2}HKMOS). The charge-compensation (CC) region introduced in C^{2}HKMOS is exploited to compensate for the influence of interface charge. This CC mechanism is also detailed analytically for $R_{on,sp}$–BV optimization.

2. Charge compensation mechanism

Figure 1 shows a cross-sectional cell unit of a C^{2}HKMOS device. At the top of the device, it is the source region, and at the bottom, it is the drain region. In the middle, the silicon drift region is connected in parallel with an HK region with a dielectric constant ε_{hk} ($\varepsilon_{hk} = k_r\varepsilon_{si}$, ε_{si} is the permittivity of silicon) and a width of w_K. The whole drift region with the width of w_N and the length of L_D consists of two parts: N-type drift region on the left and CC region with a width of w_{CC} on the right. Specially, fixed charge (viz) and interface charge (Q_{it}) exist at the hetero-interface between HK pillar and drift region. Figure 1(b) shows that the electric field displacement is absorbed by negative Q_{it}, and figure 1(c) demonstrates that the electric field displacement is repelled by positive Q_{it}.

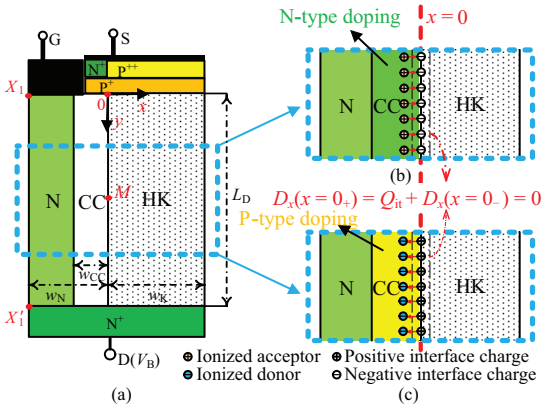


Fig. 1. Schematic digram of (a) C^{2}HKMOS, (b) CC region with N-type doping compensation, and (c) CC region with P-type doping compensation.

Based on superposition methodology,[10] the equivalent C^{2}HKMOS under the reverse-voltage sustained condition is

†Corresponding author. E-mail: zhigangwang@swjtu.edu.cn

© 2022 Chinese Physical Society and IOP Publishing Ltd

simply superposed by non-compensation CC region and extra-charge compensation CC region as shown in Fig. 2(a). The corresponding potential distribution $V_{\rm CC}(x,y)$ is equal to non-compensation potential ($V_{\rm NC}$) plus extra-charge compensation potential ($V_{\rm EC}$), *i.e.*, $V_{\rm CC}(x,y)=V_{\rm NC}(x,y)+V_{\rm EC}(x,y)$. Derivation from solving Poisson equation, $V_{\rm NC}(x,y)$ is the non-compensation potential given as

$$V_{\rm NC}(x,y)=V_{\rm B}\frac{y}{L_{\rm D}}+V_{\rm it}(x,y)+\frac{L_{\rm D}qN_{\rm NC}}{2}S_1(x,y), \tag{1}$$

$$S_1(x,y)=\begin{cases}-\dfrac{y^2}{\varepsilon_{\rm si}L_{\rm D}}+\dfrac{y}{\varepsilon_{\rm si}}+\dfrac{L_{\rm D}}{\varepsilon_{\rm si}}\displaystyle\sum_{n=\rm odd}A_1\cosh K_n(x+w_{\rm N})\sin K_ny, & -w_{\rm N}\le x<-w_{\rm CC},\\ -\dfrac{y^2}{\varepsilon_{\rm si}L_{\rm D}}+\dfrac{y}{\varepsilon_{\rm si}}+\dfrac{L_{\rm D}}{\varepsilon_{\rm si}}\displaystyle\sum_{n=\rm odd}(A_2\cosh K_nx+A_3\sinh K_nx)\sin K_ny, & -w_{\rm CC}\le x\le 0,\\ \dfrac{L_{\rm D}}{\varepsilon_{\rm hk}}\displaystyle\sum_{n=\rm odd}A_4\cosh K_n(x-w_{\rm K})\sin K_ny, & 0<x\le w_{\rm K},\end{cases} \tag{2}$$

where $K_n=n\pi/L_{\rm D}$; A_1, A_2, A_3, and A_4 are given in Eqs. (A1), (A4), (A7), and (A10) in Appendix A, respectively. $V_{\rm it}(x,y)$ is the potential yielded by the $Q_{\rm it}$ and expressed as

$$V_{\rm it}(x,y)=\sum_{m=1}^{M}N_{{\rm it},m}\sum_{n=\rm odd}C_{{\rm it},mn}\cosh K_n(x+w_{\rm N})\sin K_ny, \tag{3}$$

where $C_{{\rm it},mn}$ and $N_{{\rm it},m}$ are calculated from Eqs. (A13) and (A16) in Appendix A.

Figure 2(b) shows that in the non-compensation structure with negative $Q_{\rm it}$, the concentration of N-type drift region is $N_{\rm NC}$ and its quantity is $Q_{\rm NC}=qN_{\rm NC}w_{\rm N}$. In extra-charge compensation region, the additional charge concentration $N_{\rm EC}$ is of N-type and its quantity is $\Delta Q_{\rm EC}=qN_{\rm EC}w_{\rm CC}$. In order to achieve a uniform distribution of electric displacement in non-compensation region as shown in Fig. 2(c), $\Delta Q_{\rm EC}$ is superposed over $Q_{\rm NC}$ as a CC structure, which compensates for the disturbance of electric displacement aroused by $Q_{\rm it}$ to be horizontal in HK pillar. Intuitively, the N-type dope of $N_{\rm EC}$ compensates for the negative $Q_{\rm it}$ from Fig. 1(b), and P-type dope of $N_{\rm EC}$ compensates for the positive one from Fig. 1(c). A positive $N_{\rm CC}$ represents the ionized N-type CC region, and a negative $N_{\rm CC}$ represents the ionized P-type CC region. The extra charge yields $V_{\rm EC}(x,y)$ distribution as

$$V_{\rm EC}(x,y)=\frac{L_{\rm D}qN_{\rm EC}}{2}S_2(x,y), \tag{4}$$

$$S_2(x,y)=\begin{cases}\dfrac{L_{\rm D}}{\varepsilon_{\rm si}}\displaystyle\sum_{n=\rm odd}\frac{8\sin^2(n\pi/2)}{n^3\pi^3}A_{1,\rm CC}\cosh K_n(x+w_{\rm N})\sin K_ny, & -w_{\rm N}\le x<-w_{\rm CC},\\ -\dfrac{y^2}{\varepsilon_{\rm si}L_{\rm D}}+\dfrac{y}{\varepsilon_{\rm si}}+\dfrac{L_{\rm D}}{\varepsilon_{\rm si}}\displaystyle\sum_{n=\rm odd}\frac{8\sin^2(n\pi/2)}{n^3\pi^3}(A_{2,\rm CC}\cosh K_n+A_{3,\rm CC}\sinh K_nx)\sin K_ny, & -w_{\rm CC}\le x\le 0,\end{cases} \tag{5}$$

where $A_{1,\rm CC}$, $A_{2,\rm CC}$, and $A_{3,\rm CC}$ are given in Appendix (A3), (A6), and (A9) in Append A, respectively.

Owing to the fixed charge existing at hetero-interface between silicon pillar and HK pillar, the horizontal electric displacement is discontinuous at $x=0$ as shown in Fig. 2(c). At $x=0$, the horizontal electric displacement is discontinuous. The difference in electric displacement between $x=0_+$ and $x=0_-$ satisfies $D_x(x=0_+)-D_x(x=0_-)=Q_{\rm it}$. The horizontal electric displacement $D_{x,\rm CC}(x,y)$ is superposed by non-compensation one- $D_{x,\rm NC}(x,y)$ and extra-charge compensated one- $D_{x,\rm EC}(x,y)$ given as

$$D_{x,\rm CC}(x,y)=D_{x,\rm NC}(x,y)+D_{x,\rm EC}(x,y), \tag{6}$$

In light of Eq. (1), $D_{x,\rm NC}(x,y)$ is expressed as

$$D_{x,\rm NC}(x,y)=\varepsilon_{\rm si}\times\left(\frac{{\rm d}V_{\rm it}(x,y)}{{\rm d}x}+\frac{L_{\rm D}qN_{\rm NC}}{2}\frac{{\rm d}S_1(x,y)}{{\rm d}x}\right). \tag{7}$$

According to Eq. (1), $D_{x,\rm EC}(x,y)$ is obtained as

$$D_{x,\rm EC}(x,y)=\varepsilon_{\rm si}\times\left(\frac{L_{\rm D}qN_{\rm EC}}{2}\frac{{\rm d}S_2(x,y)}{{\rm d}x}\right). \tag{8}$$

It is obviously found from Fig. 2(c) that the electric displacement yielded by extra-charge can offset the electric displacement yielded by non-compensation in HK region to uniform electric field in Fig. 2(d). After compensation, $D_x(x,y)$ in HK region equals zero. In order to verify this mechanism, figure 3 shows the verification of the horizontal electric displacement along line M_1–M–M_2 at $y=L_{\rm D}/2$. In the conventional HKMOS (CHKMOS) without $Q_{\rm it}$, the D_x at $y=L_{\rm D}/2$ demonstrates a triangle distribution and the D_x peak appears at point M. Nonetheless, in the CHKMOS with negative $Q_{\rm it}$, a negative D_x peak is at $x=0_-$ and a positive one is at $x=0_+$ due to the existence of $Q_{\rm it}$. As shown in Fig. 3(a), the negative $Q_{\rm it}$ ($N_{\rm it}=-1.0\times10^{12}$ cm^{-2}) results in $D_x(0_+)<0$. The extra-charge in CC region is presened by ionized donor, and the

charge density is $N_{\rm EC} = 3.33 \times 10^{15}$ cm^{-3}. After imbedding CC region into C^{2}HKMOS, the electric displacement in the HK is modified into being horizontal. Conversely, in Fig. 3(b), C^{2}HKMOS with the positive $Q_{\rm it}$ ($N_{\rm it} = 1.0 \times 10^{12}$ cm^{-2}) results in $D_x(0_+) > 0$. The extra-charge in P-type CC region is ionized acceptor, and its density is $N_{\rm EC} = -1.5 \times 10^{16}$ cm^{-3} to flatten the electric displacement to zero in HK pillar.

Assuming that $D_x(0_+) = 0$, the extra-charge concentration $N_{\rm EC}$ reaches the optimal value to guarantee an uniform electric field along X_1–X_1' as schematically shown in Fig. 2(d) and verified in Fig. 3. Derived from the formula (6), the optimal $N_{\rm EC}$ is

$$N_{\rm EC} = -\left(\frac{N_{\rm NC}}{\alpha} + \frac{N_{\rm it}}{w_{\rm CC}\beta}\right), \tag{9}$$

where the coefficients α and β are given as

$$\alpha = \frac{\sum\limits_{n=\rm odd} K_n A_{3,\rm CC} \sin(n\pi/2)}{\sum\limits_{n=\rm odd} K_n (A_{3,\rm N} + A_{3,\rm CC}) \sin(n\pi/2)}, \tag{10}$$

$$\beta = \frac{\sum\limits_{m=1}^{M} N_{{\rm it},m} W_{{\rm it},m} \sum\limits_{n=\rm odd} \varepsilon_{\rm si} K_n A_{3,\rm CC} \sin(n\pi/2)}{\sum\limits_{m=1}^{M} \sum\limits_{n=\rm odd} \varepsilon_{\rm si} w_{\rm CC} L_{\rm D} N_{{\rm it},m} C_{{\rm it},mn} K_n \sinh K_n w_{\rm N} \sin(n\pi/2) - q \sum\limits_{m=1}^{M} w_{\rm CC} N_{{\rm it},m} W_{{\rm it},m}}, \tag{11}$$

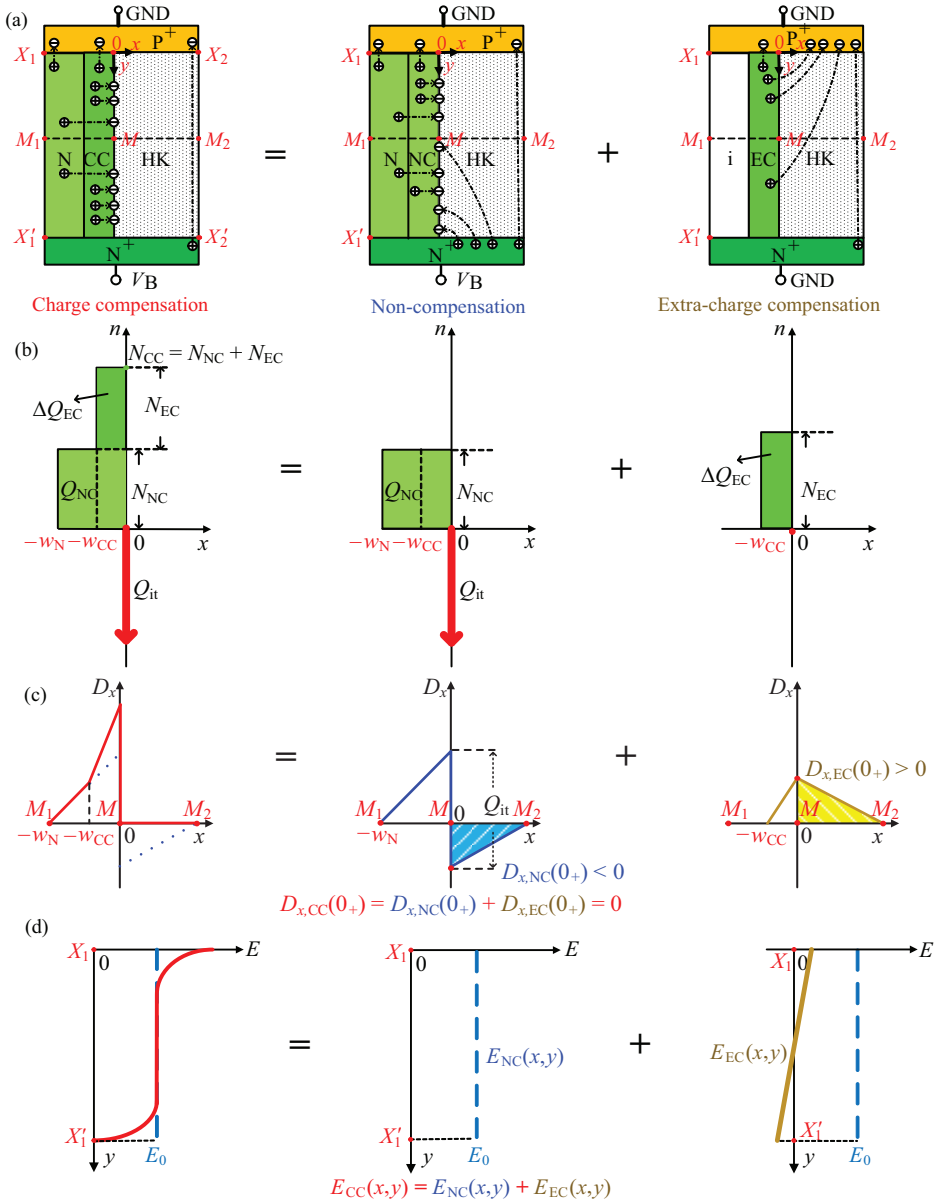


Fig. 2. Superposition method used in deriving electric displacement of C^{2}HKMOS: (a) schematic equivalent diagram of C^{2}HKMOS by superposition, (b) equivalent charge concentration, (c) compensation of electric displacement, and (d) superposition of the electric field. In panel (a), the CC structure is split into a non-compensation one and extra-charge compensation one. After compensation, the horizontal electric displacement in HK pillar is modulated to be zero in panel (c) and electric field distributes uniformly along X_1–X_1' in panel (d).

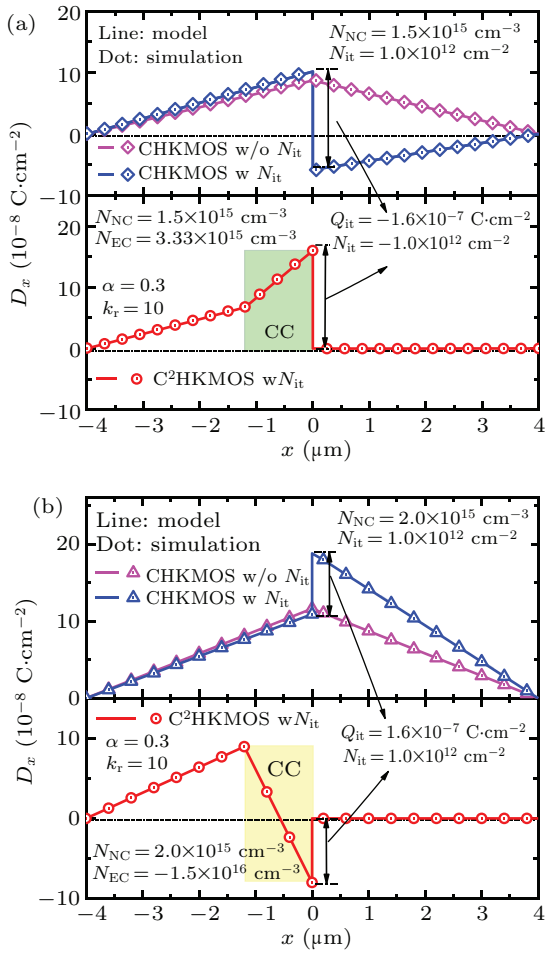


Fig. 3. D_x along line M_1–M–M_2: (a) compensation for negative Q_{it} with $N_{it}=-1.0\times10^{12}$ cm^{-2} and (b) compensation for positive Q_{it} with $N_{it}=1.0\times10^{12}$ cm^{-2}. At the hetero-interface in panels (a) and (b), the fixed Q_{it} results in abrupt change of electric displacement, and ionized charge in CC region can change electric displacement into being horizontal in HK pillar. The abbreviations "w" and "w/o" in the figure express "with" an "without", respectively.

where parameter $K_n=n\pi/L_D$, N_{it} is the Q_{it} density, parameter $A_{3,N}$ and $A_{3,CC}$ are shown in Eqs. (A8) and (A9) of Appendix A.

In the C^{2}HKMOS, according to Gauss law,[18] the flux integral of the electric displacement along close path X_1–X_1'–X_2'–X_2 is

$$\oint_{X_1X_1'X_2'X_2} D(x,y)\mathrm{d}x\mathrm{d}y = Q_{NC}+\Delta Q_{EC}+Q_{it}. \tag{12}$$

There is no doubt that in Eq. (12) the right term equal to zero causes the left term to appear in the form of symmetric distribution, similar to superjuction or PIN diode. As indicated in Fig. 2(d), the optimized electric field needs to be as close to the ideal PIN diode as possible to maximize BV. It implies that the uniform $D(x,y)$ along the line X_1–X_1' and the line X_2–X_2' with $D_x(x,y)=0$ is illustrated at $x=\pm4$ μm in Fig. 3. Hence, the limited condition is simplified from Eq. (9) into

$$qw_{CC}\left(\frac{N_{NC}}{\alpha}+N_{EC}+\frac{N_{it}}{w_{CC}\beta}\right)=Q_{NC}+\Delta Q_{EC}+Q_{it}\approx 0. \tag{13}$$

It is worth pointing out that using the numerical calculation, the value of β is approximately 1, *i.e.*, $\beta\approx1$ with a deviation $<1\%$ after electric-displacement compensation. From Fig. 4, it is available that α demonstrates a linear function of w_{CC} and can be expressed approximately as $\alpha\approx w_{CC}/w_N$. Equation (13) implies an approximation of charge-balance condition for contracting electric flux to attain $D_x(0_+)=0$. Note that extra charge satisfies Eq. (13) with little influence from k_r and L_D.

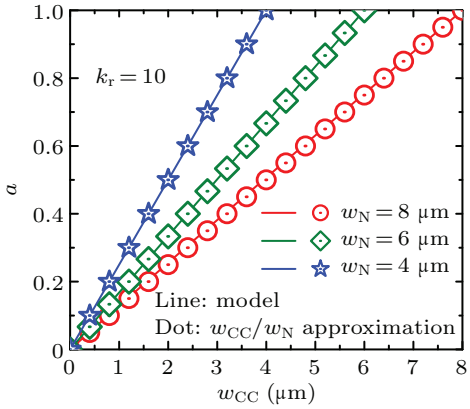


Fig. 4. Curves of α *versus* w_{CC} for $k_r=10$ and $w_N=4$, 6, 8 μm, indicating that α varies linearly with w_{CC}.

3. Optimization of breakdown voltage

In the C^{2}HKMOS, the electric displacement along the line X_1–X_1' is derived from Eq. (1) as

$$\begin{aligned}
&D(x=-w_N,y)\\
&=\varepsilon_{si}\times\left\{\frac{V_B}{L_D}+\frac{L_D qN_{NC}}{2}\right.\\
&\times\left[1-\frac{2y}{L_D}+\sum_{n=\text{odd}}\frac{8\sin^2(n\pi/2)}{n^2\pi^2}(A_{1,N}+A_{1,CC})\cos K_n y\right]\\
&+\sum_{m=1}^{M}N_{it,m}\sum_{n=\text{odd}}B_{it,mn}K_n\cos K_n y+\frac{L_D qN_{EC}}{2}\\
&\left.\times\sum_{n=\text{odd}}\frac{8\sin^2(n\pi/2)}{n^2\pi^2}A_{1,CC}\cos K_n y\right\}.
\end{aligned}\tag{14}$$

After compensation, the whole drift region is under punch-through and the avalanche breakdown location retains at point X_1. At this location, the electric displacement is

$$D(-w_N,0)=D_0+D_1(-w_N,0)+D_{EC}(-w_N,0), \tag{15}$$

where $D_0=\varepsilon_{si}V_B/L_D$ and $D_{EC}(x,y)$ donates the additional electric displacement caused by the compensation charge N_{EC}. At avalanche breakdown, the electric displacement along line X_1–X_1' is approximated by

$$D(-w_N,y)=D_0(1+\lambda\exp(-2y/L_D\zeta), \tag{16}$$

where, $\lambda=D_2/D_0$, $\zeta=D_2/(\varepsilon_{si}N_{NC})$, and $D_2=D_1(-w_N,0)+D_{EC}(-w_N,0)$. From Fulop's model,[19] ionization integral in $D(y)$ form is $\int 1.25268\times10^{49}D(-w_N,y)^7\mathrm{d}y=$

1. Submitting $D(-w_N, y)$ into ionization integral, we find that

$$1.31926\times10^{37}D_0^6BV=(1+\xi)^{-1}, \tag{17}$$

where $\xi=\zeta\cdot F(\lambda)/840$, and $F(\lambda)=\lambda(2940+\lambda(4410+\lambda(4900+\lambda(3675+2\lambda(882+5\lambda(49+6\lambda))))))$. In $F(\lambda)$, $\lambda=0$ is obtained in the ideal PIN diode. The BV of ideal PIN diode is recorded as $BV_{\rm PIN}$.[9,10] So assuming $\lambda=0$, equation (17) becomes

$$1.31926\times10^{37}\left(\frac{\varepsilon_{\rm si}}{L_{\rm D}}\right)^6 BV_{\rm PIN}^7=1. \tag{18}$$

Considering the case in Eq. (18) and eliminating $L_{\rm D}$, the normalized factor $\eta=BV/BV_{\rm PIN}$ is calculated by

$$\eta=(1+\xi)^{-1/7}, \tag{19}$$

$$L_{\rm D}=1.62\times10^{-6}\eta^{-7/6}BV^{7/6}. \tag{20}$$

For the ideal PIN diode, $\eta=1$ substituted into Eq. (20) is for the ideal drift region length, $L_{\rm D(ideal)}=1.62\times10^{-6}\ BV^{7/6}$, and for the C^{2}HKMOS, $\eta\approx0.959$ yields the optimized drift region length $L_{\rm D(opt)}=1.70\times10^{-6}\ BV^{7/6}$. According to $\eta\approx0.959$ in the C^{2}HKMOS, the optimized $L_{\rm D}$ is calculated at given BV. In Fig. 5, the red dotted line represents $L_{\rm D}$–BV curve of ideal PIN at $\gamma=0$ from Eq. (20). In Fig. 5(a), the C^{2}HKMOS with $N_{\rm it}=-1.0\times10^{12}$ cm^{-2} shows that at the same BV, a smaller α means a higher dosage in N-type CC region to ensure minimized $L_{\rm D}$ approaching to the PIN limit. In Fig. 5(b), the C^{2}HKMOS with $N_{\rm it}=1.0\times10^{12}$ cm^{-2} shows that at the same BV, the larger α needs a wider P-type CC region and smaller$N_{\rm EC}$. Comparing with CHKMOS without $Q_{\rm it}$, the $L_{\rm D}$–BV relation of C^{2}HKMOS can approach to the PIN limit as much as possible.

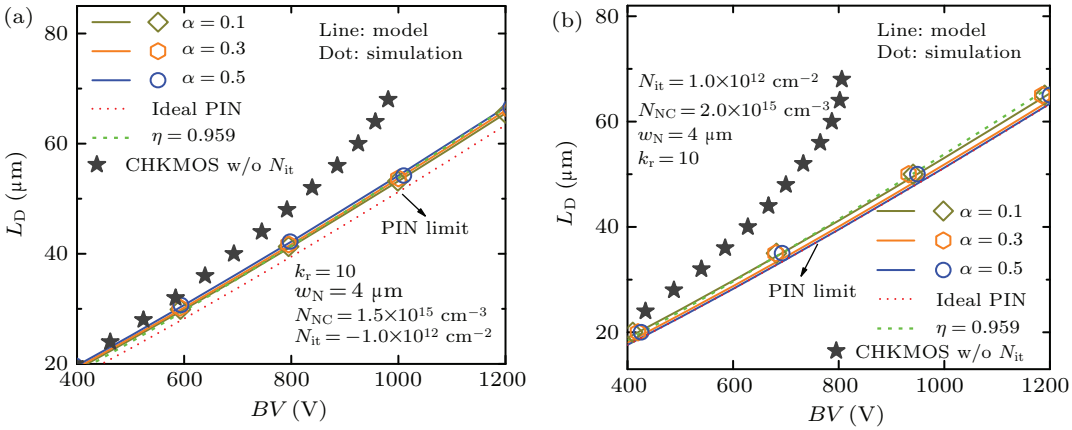


Fig. 5. Values of optimized $L_{\rm D}$ *versus* BV at various values of α, showing the smaller the width $w_{\rm CC}$, the closer to the PIN limit the value of$L_{\rm D}$ is, (a) for negative $Q_{\rm it}$ with $N_{\rm it}=-1.0\times10^{12}$ cm^{-2}, and (b) for positive $Q_{\rm it}$ with $N_{\rm it}=1.0\times10^{12}$ cm^{-2}. This case is much closer to the scenario of PIN limit.

4. Optimization of specific ON-resistance

The calculation of $R_{\rm on,sp}$ in the C^{2}HKMOS needs to take JFET into account like superjunction.[20–22] After BV design as aforementioned in Section 3, the $Q_{\rm it}$ is compensated for by CC region. In Fig. 6(a), the $Q_{\rm it}$ is negative. So the CC region is chosen to be an N-type region with a concentration of $N_{\rm CC}$. However, in Fig. 6(b), the positive interface needs a P-type CC region. When the C^{2}HKMOS is at ON-state, the source potential is grounded, and the drain potential is $V_{\rm DS}$. The CC region is unintentionally depleted for generating JFET effect.

For the negative $Q_{\rm it}$, the conduction resistance in C^{2}HKMOS includes two parts, *i.e.*, R_1 and R_2, and expressed respectively as

$$R_1=\frac{L_{\rm D}}{\mu_1M_1}=\frac{L_{\rm D}}{\mu_1qN_{\rm NC}(w_{\rm N}-w_{\rm CC})}, \tag{21}$$

$$R_2=\frac{L_{\rm D}}{\mu_2M_2}=\frac{L_{\rm D}}{\mu_2(qN_{\rm CC}w_{\rm CC}-\sqrt{4q\varepsilon_{\rm si}N_{\rm CC}\varphi_{\rm fn}})}, \tag{22}$$

where M_1 is the electron density in the N region, M_2 is the electron density of the CC region with JFET taken into account caused by $Q_{\rm it}$, μ_1 and μ_2 are carrier mobilities in Eqs. (A17) and (A18), respectively. The Fermi potential $\varphi_{\rm fn}$ is

$$\varphi_{\rm fn}=V_{\rm t}\ln(N_{\rm CC}/n_{\rm i}), \tag{23}$$

where $V_{\rm t}$ is the thermal voltage and n_i is the intrinsic carrier concentration.

In the case of Fig. 6(a), the total $R_{\rm on,sp,n}$ is composed of parallel resistance R_1 and R_2 as

$$\begin{aligned}R_{\rm on,sp,n}&=\frac{R_1R_2}{R_1+R_2}\times(w_{\rm N}+w_{\rm K})\\&=\frac{2L_{\rm D}}{q}\cdot\left(\mu_1N_{\rm NC}(1-\alpha)+\mu_2N_{\rm CC}\alpha-\frac{\sqrt{2V_{\rm t}\varepsilon_{\rm si}}}{w_{\rm N}}\right.\\&\left.\times\mu_2\sqrt{N_{\rm CC}\ln\left(\frac{N_{\rm CC}^2}{n_i^2}\right)}\right)^{-1}.\end{aligned} \tag{24}$$

In the case of Fig. 6(b), the total electron density for conduction G_n is $G_{\rm n}=qN_{\rm NC}(w_{\rm N}-w_{\rm CC})-\sqrt{2q\varepsilon_{\rm si}N_0\varphi_{\rm bi}}$, where $N_0=N_{\rm NC}\cdot|N_{\rm CC}|/(N_{\rm NC}+|N_{\rm CC}|)$, and the built-in potential is $\varphi_{\rm bi}=V_{\rm t}\cdot\ln(|N_{\rm CC}|N_{\rm NC}/n_i^2)$. So, $R_{\rm on,sp,p}$ is derived as

$$R_{\rm on,sp,p}=R_3\times(w_{\rm N}+w_{\rm K})=\frac{L_{\rm D}}{\mu_1G_{\rm n}}\times(w_{\rm N}+w_{\rm K})$$

$$= \frac{2L_{\rm D}}{q}\cdot\left(\mu_1 N_{\rm NC}(1-\alpha)-\frac{\sqrt{2V_{\rm t}\varepsilon_{\rm si}}}{w_{\rm N}}\right.$$
$$\left.\times\mu_1\sqrt{N_0\ln\left(\frac{|N_{\rm CC}|N_{\rm NC}}{n_i^2}\right)}\right)^{-1}. \quad (25)$$

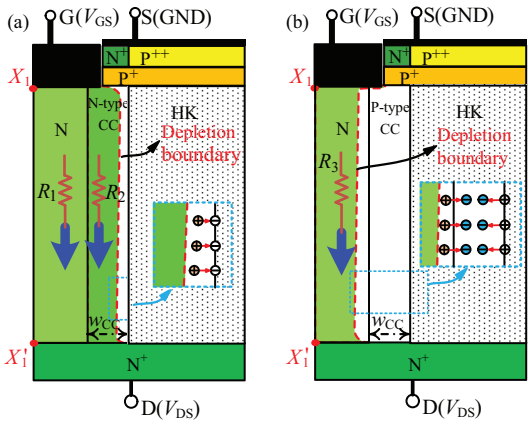


Fig. 6. Schematics of conduction channel in C^{2}HKMOS (a) with negative $Q_{\rm it}$ and N-doped CC region, and (b) with positive $Q_{\rm it}$ and P-doped CC region, where dashed line denotes depletion boundary due to JFET effect caused by $Q_{\rm it}$.

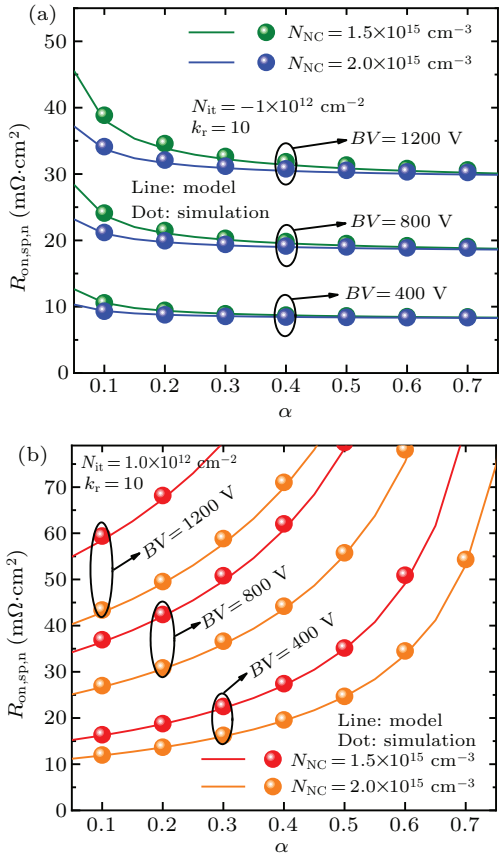


Fig. 7. Curves of $R_{\rm on,sp}$ *versus* α of C^{2}HKMOS at $BV=400$ V, 800 V, and 1200 V: (a) $R_{\rm on,sp,n}$–α curve with $N_{\rm it}=-1.0\times10^{12}$ cm^{-2}, and (b) $R_{\rm on,sp,p}$–α curve with $N_{\rm it}=1.0\times10^{12}$ cm^{-2}.

Figure 7 shows $R_{\rm on,sp,n}/R_{\rm on,sp,p}$ of C^{2}HKMOS *versus* α at $BV=400$ V–1200 V in steps of 400 V. As indicated in Eq. (24), a chosen $N_{\rm NC}$ needs $N_{\rm CC}$ to be optimized in CC region to compensate for $R_{\rm on,sp,n}$ into a small value as shown in Fig. 7(a). Eventually, in the case of Fig. 7(b), the increasing α results in enlarging $R_{\rm on,sp,p}$, which is mainly attributed to the reduction of conduction path with limited modification in Eq. (25).

Figure 8 shows the curves of $R_{\rm on,sp}$ *versus* $N_{\rm NC}$ in various cases, demonstrating that at small variation of BV, α, and $N_{\rm NC}$ can be quickly optimized to achieve $R_{\rm on,sp,n(opt)}$ for the same value. This method means that for a given C^{2}HKMOS, optimized $R_{\rm on,sp,n(opt)}$ is easily obtained by CC.

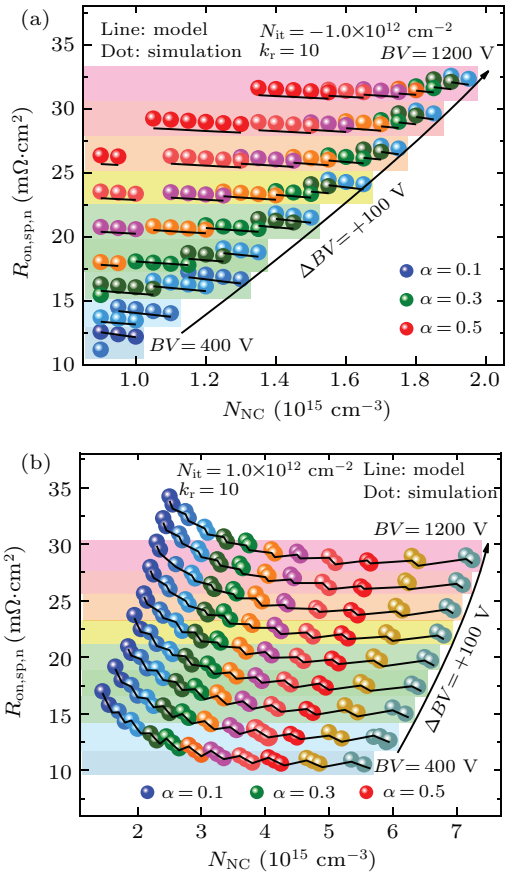


Fig. 8. Curves of $R_{\rm on,sp}$ *versus* $N_{\rm NC}$ at optimization in C^{2}HKMOS, showing (a) $R_{\rm on,sp,n}$–$N_{\rm NC}$ curve with $N_{\rm it}=-1.0\times10^{12}$ cm^{-2} and (b) $R_{\rm on,sp,p}$–$N_{\rm NC}$ curve with $N_{\rm it}=1.0\times10^{12}$ cm^{-2}. The color bands represent the same values of BV for a certain value of $L_{\rm D}$. $N_{\rm NC}$ and $N_{\rm CC}$ as the parameters are optimized for minimizing $R_{\rm on,sp}$.

5. Optimization method

The optimization process of $R_{\rm on,sp}$–BV trade-off is estimated as follows.

(i) At a given targeted BV, the range of $L_{\rm D}$ is achieved from Eq. (20). This BV approaches to the limit of PIN diode to achieve minimum $L_{\rm D}$ by charge compensation in internal relation of doping concentration, whereas the relation between $N_{\rm CC}$ and $N_{\rm EC}$, which is associated with α, is realized via Eq. (9) profiting from $D_x=0$ in the HK region.

(ii) In order to minimize $R_{\rm on,sp}$, the evaluation of $N_{\rm CC}$ and $N_{\rm EC}$ should be further determined in a small range. Hence, the optimization of $N_{\rm CC}$, $N_{\rm EC}$, and α is an eventual target for $R_{\rm on,sp}$–BV trade-off. Simplifying Eqs. (24) and (25), $R_{\rm on,sp}$–BV trade-off is uniformly rewritten as

$$R_{\rm on,sp}=2.12636\times10^{13}BV^{1.167}f^{-1}, \quad (26)$$

$$f^{-1}=\begin{cases}\mu_1 N_{\rm NC}(1-\alpha)+\mu_2 N_{\rm CC}-787\mu_2 w_{\rm N}^{-1}N_{\rm CC}^{0.5369}, & N_{\rm it}<0,\\ \mu_1 N_{\rm NC}(1-\alpha)-1428\mu_1 w_{\rm N}^{-1}N_0^{0.5211}, & N_{\rm it}>0.\end{cases} \tag{27}$$

According to forward steps, in a range of 400 V $\leq BV \leq$ 1200 V and 2 μm $\leq w_{\rm N} \leq$ 6 μm, the design parameters $N_{\rm CC}$ and α with negative $Q_{\rm it}$ are fitted into power function as

$$\begin{cases}\alpha_{\rm n,opt}=9.9339\times10^{11}w_{\rm N}^{-1.064}(-N_{\rm it})^{-1.5864}BV^{1.0354},\\ N_{\rm CC,n,opt}=1.6423\times10^{-10}w_{\rm N}^{0.2801}(-N_{\rm it})^{2.4863}BV^{-1.1662}.\end{cases} \tag{28}$$

Table 1. Key data in optimization ($w_{\rm N}=4$ μm).

BV (V)	$N_{\rm it}$ (10^{12} cm^{-2})	α	$N_{\rm CC}$ (10^{15} cm^{-3})	$R_{\rm on,sp,mod}$ (mΩ·cm^2)	$R_{\rm on,sp,sim}$ (mΩ·cm^2)
400	–1.2	0.1	21.9	10.59	10.63
	–1	0.12	14.23	11.79	12.03
	–0.8	0.18	7.01	13.03	13.07
	0.8	0.6	–6.7	11.38	11.57
	1	0.65	–7.32	10.35	10.4
	1.2	0.65	-8.41	9.48	9.52
800	–1.2	0.31	7.67	17.76	18.16
	–1	0.4	4.9	20.38	20.75
	–0.8	0.55	2.82	24.39	24.61
	0.8	0.6	–7.4	20.95	21.27
	1	0.6	–8.57	19.41	19.7
	1.2	0.55	–10.53	18.15	18.45
1200	–1.2	0.44	5.67	26.96	27.25
	–1	0.56	3.68	31.21	31.78
	–0.8	0.95	2.01	37.43	37.92
	0.8	0.5	–9.3	30.11	30.11
	1	0.5	–10.65	28.31	28.29
	1.2	0.5	-12	26.7	26.67

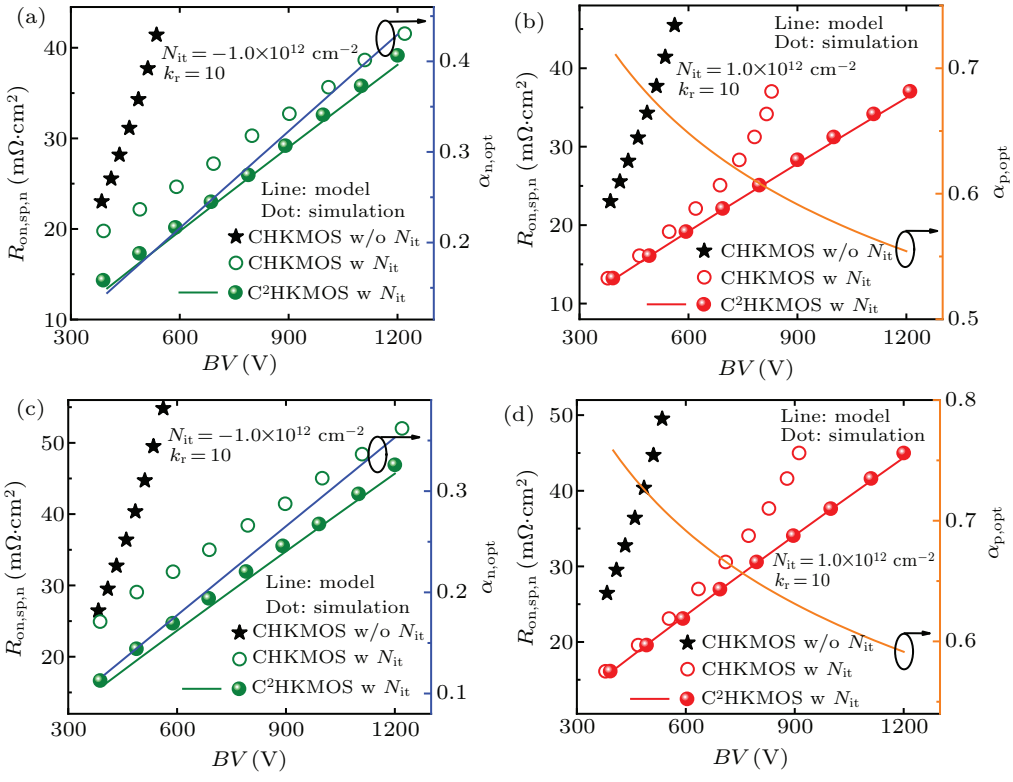


Fig. 9. Curves of $R_{\rm on,sp}$–BV trade-off (a) at $N_{\rm it}=-1.0\times10^{12}$ cm^{-2} and $w_{\rm N}=5$ μm, (b) at $N_{\rm it}=1.0\times10^{12}$ cm^{-2} and $w_{\rm N}=5$ μm, (c) at $N_{\rm it}=-1.0\times10^{12}$ cm^{-2} and $w_{\rm N}=6$ μm, and (d) at $N_{\rm it}=1.0\times10^{12}$ cm^{-2} and $w_{\rm N}=6$ μm.

For the optimized Eq. (28), the corresponding optimized $R_{\mathrm{on,sp,n}}$ is also given as

$$R_{\mathrm{on,sp,n,opt}} = 1.9938\times10^{11} w_{\mathrm{N}}^{0.9858}(-N_{\mathrm{it}})^{-0.7841} BV^{0.9571}. \quad (29)$$

In the same steps for C^{2}HKMOS with positive interface in a range of 400 V $\le BV \le$ 1200 V and 2 μm $\le w_{\mathrm{N}} \le$ 6 μm,, the optimized N_{CC}, α, and $R_{\mathrm{on,sp,n}}$ are achieved as

$$\begin{cases} \alpha_{\mathrm{p,opt}} = 0.8946\times w_{\mathrm{N}}^{0.3562} N_{\mathrm{it}}^{0.1387} BV^{-0.2262}, \\ N_{\mathrm{CC,p,opt}} = -2572\times w_{\mathrm{N}}^{-1.5299} N_{\mathrm{it}}^{0.5155} BV^{0.4017}, \end{cases} \quad (30)$$

$$R_{\mathrm{on,sp,p,opt}} = 2.8117\times10^{6} w_{\mathrm{N}}^{1.1139} N_{\mathrm{it}}^{-0.3358} BV^{0.9147}. \quad (31)$$

The key data are given in Table 1 in calibration. According to optimization method, the $R_{\mathrm{on,sp}}$–BV trade-off by Eqs. (29) and (31) is illustrated in Fig. 9. Figures 9(a) and 9(c) represent$R_{\mathrm{on,sp}}$–BV curves in the case of Fig. 6(a). The negative Q_{it} compensated by CC region can enhance the total doping concentration in the drift region for lowering $R_{\mathrm{on,sp}}$. However, as shown in Figs. 9(b) and 9(d), the C^{2}HKMOS with positive Q_{it} demonstrates that the CC region is introduced mainly into the smooth electric displacement to avoid degenerating the BV. With the increase of w_{N} with respect to the ratio of $\Delta Q_{\mathrm{EC}}/Q_{\mathrm{NC}}$, N-type CC region, and P-type CC region show the enhancement of $R_{\mathrm{on,sp}}$-BV trade-off in comparison with the CHKMOS.

6. Conclusions

For the quick designing of HKMOS with Q_{it}, an analytical model is developed by the CC theory for the first time. This model reveals the CC mechanism from the angle of superposition byh modifying the electric displacement, and also predicts the BV limit. In addition, the C^{2}HKMOS with negative and the C^{2}HKMOS with positive Q_{it} are both thoroughly established to calculate $R_{\mathrm{on,sp}}$ with JFET effect taken into account. A simple and effective method is proposed to mitigate $R_{\mathrm{on,sp}}$–BV trade-off by adding the N-type or P-type CC region into HKMOS. The model results and simulation results are shown to be in agreement between each other.

Acknowledgements

Project supported by the National Natural Science Foundation of China (Grant No. 61404110) and the National Higher-education Institution General Research and Development Project (Grant No. 2682014CX097).

Appendix A: Expressions of A in Eq. (2)

$$A_1 = \frac{8\sin^2(n\pi/2)}{n^3\pi^3}(N_{\mathrm{NC}}A_{1,\mathrm{N}}+N_{\mathrm{CC}}A_{1,\mathrm{CC}}). \quad (A1)$$

$$A_{1,\mathrm{N}} = -\frac{k_{\mathrm{r}}\cosh K_n w_{\mathrm{CC}}\sinh K_n w_{\mathrm{K}}+\cosh K_n w_{\mathrm{K}}\sinh K_n w_{\mathrm{CC}}}{\cosh K_n w_{\mathrm{K}}\sinh K_n w_{\mathrm{N}}+k_{\mathrm{r}}\cosh K_n w_{\mathrm{N}}\sinh K_n w_{\mathrm{K}}}. \quad (A2)$$

$$A_{1,\mathrm{CC}} = -\frac{k_{\mathrm{r}}(1-\cosh K_n w_{\mathrm{CC}})\sinh K_n w_{\mathrm{K}}-\cosh K_n w_{\mathrm{K}}\sinh K_n w_{\mathrm{CC}}}{\cosh K_n w_{\mathrm{K}}\sinh K_n w_{\mathrm{N}}+k_{\mathrm{r}}\cosh K_n w_{\mathrm{N}}\sinh K_n w_{\mathrm{K}}}. \quad (A3)$$

$$A_2 = \frac{8\sin^2(n\pi/2)}{n^3\pi^3}(N_{\mathrm{NC}}A_{2,\mathrm{N}}+N_{\mathrm{CC}}A_{2,\mathrm{CC}}). \quad (A4)$$

$$A_{2,\mathrm{N}} = \frac{\cosh K_n w_{\mathrm{K}}\sinh K_n(w_{\mathrm{N}}-w_{\mathrm{CC}})}{\cosh K_n w_{\mathrm{K}}\sinh K_n w_{\mathrm{N}}+k_{\mathrm{r}}\cosh K_n w_{\mathrm{N}}\sinh K_n w_{\mathrm{K}}}. \quad (A5)$$

$$A_{2,\mathrm{CC}} = -\frac{k_{\mathrm{r}}\cosh K_n(w_{\mathrm{N}}-w_{\mathrm{CC}})\cosh K_n w_{\mathrm{CC}}\sinh K_n w_{\mathrm{K}}}{\cosh K_n w_{\mathrm{K}}\sinh K_n w_{\mathrm{N}}+k_{\mathrm{r}}\cosh K_n w_{\mathrm{N}}\sinh K_n w_{\mathrm{K}}} - \frac{(\cosh K_n w_{\mathrm{K}}+k_{\mathrm{r}}\sinh K_n w_{\mathrm{CC}}\sinh K_n w_{\mathrm{K}})\sinh K_n(w_{\mathrm{N}}-w_{\mathrm{CC}})}{\cosh K_n w_{\mathrm{K}}\sinh K_n w_{\mathrm{N}}+k_{\mathrm{r}}\cosh K_n w_{\mathrm{N}}\sinh K_n w_{\mathrm{K}}}. \quad (A6)$$

$$A_3 = \frac{8\sin^2(n\pi/2)}{n^3\pi^3}(N_{\mathrm{NC}}A_{3,\mathrm{N}}+N_{\mathrm{CC}}A_{3,\mathrm{CC}}), \quad (A7)$$

$$A_{3,\mathrm{N}} = -\frac{k_{\mathrm{r}}\sinh K_n w_{\mathrm{K}}\sinh K_n(w_{\mathrm{N}}-w_{\mathrm{CC}})}{\cosh K_n w_{\mathrm{K}}\sinh K_n w_{\mathrm{N}}+k_{\mathrm{r}}\cosh K_n w_{\mathrm{N}}\sinh K_n w_{\mathrm{K}}}. \quad (A8)$$

$$A_{3,\mathrm{CC}} = -\frac{k_{\mathrm{r}}\sinh K_n w_{\mathrm{K}}(\sinh K_n w_{\mathrm{N}}-\sinh K_n(w_{\mathrm{N}}-w_{\mathrm{CC}}))}{\cosh K_n w_{\mathrm{K}}\sinh K_n w_{\mathrm{N}}+k_{\mathrm{r}}\cosh K_n w_{\mathrm{N}}\sinh K_n w_{\mathrm{K}}}. \quad (A9)$$

$$A_4 = \frac{8\sin^2(n\pi/2)}{n^3\pi^3}(N_{\mathrm{NC}}A_{4,\mathrm{N}}+N_{\mathrm{CC}}A_{4,\mathrm{CC}}), \quad (A10)$$

$$A_{4,\mathrm{N}} = \frac{\sec hK_n w_{\mathrm{K}}\sinh K_n(w_{\mathrm{N}}-w_{\mathrm{CC}})}{\sinh K_n w_{\mathrm{N}}+k_{\mathrm{r}}\cosh K_n w_{\mathrm{N}}\tanh K_n w_{\mathrm{K}}}. \quad (A11)$$

$$A_{4,\mathrm{CC}} = \frac{\sec hK_n w_{\mathrm{K}}(\sinh K_n w_{\mathrm{N}}-\sinh K_n(w_{\mathrm{N}}-w_{\mathrm{CC}}))}{\sinh K_n w_{\mathrm{N}}+k_{\mathrm{r}}\cosh K_n w_{\mathrm{N}}\tanh K_n w_{\mathrm{K}}}, \quad (A12)$$

$$C_{\mathrm{it},mn} = \frac{qL_{\mathrm{D}}}{2\varepsilon_{\mathrm{si}}}B_{\mathrm{it},mn}. \quad (A13)$$

$$B_{\mathrm{it},mn} = \frac{8\sin K_n\dfrac{W_{\mathrm{it},m}}{2}\sin K_n y_m}{n^2\pi^2(1+k_{\mathrm{r}}\tanh K_n w_{\mathrm{K}}\coth K_n w_{\mathrm{N}})\sinh K_n w_{\mathrm{N}}}. \quad (A14)$$

The distribution of Q_{it} is usually uneven. The Q_{it} window is divided into M parts. The midpoint of the N-th window is

y_m, corresponding to the density $N_{\mathrm{it},m}$ of each part, the width $W_{\mathrm{it},m}$ of each part described as[10]

$$W_{\mathrm{it},1} = \cdots = W_{\mathrm{it},m} = \cdots = W_{\mathrm{it},M} = W_{\mathrm{it}}/M. \tag{A15}$$

Arbitrarily distributed Q_{it} average density N_{it} is

$$N_{\mathrm{it}} = \frac{1}{L_{\mathrm{D}}} \sum_{m=1}^{M} N_{\mathrm{it},m} W_{\mathrm{it},m}. \tag{A16}$$

The carrier mobility in the N-type drift region is

$$\mu_1 = 52.2 + \frac{1364}{1 + 2.82 \times 10^{-12} N_{\mathrm{NC}}^{0.68}}. \tag{A17}$$

The carrier mobility in the N-type CC region is

$$\mu_2 = 52.2 + \frac{1364}{1 + 2.82 \times 10^{-12} N_{\mathrm{CC}}^{0.68}}. \tag{A18}$$

References

[1] Wang Y, Wang Z, Bai T and Kuo J B 2018 *Trans. Electron Dev.* **65** 1056

[2] Mao S J, Zhu Z Y, Wang G L, Zhu H L, Li J F and Zhao C 2016 *Chin. Phys. Lett.* **33** 118502

[3] Yao J F, Guo Y F, Zhang Z Y, Yang K M, Zhang M L and Xia T 2020 *Chin. Phys. B* **29** 038503

[4] Wu L J, Zhang Z J, Song Y, Yang H, Hu L M and Yuan N 2017 *Chin. Phys. B* **26** 027101

[5] Wang C L and Sun J 2009 *Chin. Phys. B* **18** 1231

[6] Chen X and Huang M 2012 *Trans. Electron Dev.* **59** 2430

[7] Huang J Q, He W W, Chen J, Luo J X, Lu K and Chai Z 2016 *Chin. Phys. Lett* **33** 096101

[8] Guan H, Lv H L, Guo H, Zhang Y M, Zhang Y M and Wu L F 2015 *Chin. Phys. B* **24** 126701

[9] Wang Z, Wang X and Kuo J B 2018 *Trans. Electron Dev.* **65** 4947

[10] Zhang W, Zhang B, Qiao M, Luo X and Li Z 2016 *Trans. Electron Dev.* **64** 224

[11] Chen X, Wang Z, Wang X and Kuo J B 2018 *Chin. Phys. B* **27** 048502

[12] Qi L W, Meng J, Liu X Y, Weng Y, Liu Z C, Zhang D H, Zhou J T and Jin Z 2020 *Chin. Phys. B* **29** 104212

[13] Hu S, Yang L, Mi M H, Hou B, Liu S, Zhang M, Wu M, Zhu Q, Wu S, Lu Y, Zhu J J, Zhou X W, Lv L, Ma X H and Hao Y 2020 *Chin. Phys. B* **29** 087305

[14] Wang Z G, Zhang B, Fu Q, Xie G and Li Z J 2012 *IEEE Electron Dev. Lett.* **33** 703

[15] Ren M, Li Z H, Deng G M, Zhang L X, Zhang M, Liu X L, Xie J X and Zhang B 2012 *Chin. Phys. B* **21** 048502

[16] Huang H, Xu S, Xu W, Hu K, Cheng J, Hu H and Yi B 2020 *Trans. Electron Dev.* **67** 2463

[17] Huang H, Hu K, Xu W, Xu S, Cui W, Zhang W and Ng W T 2020 *Trans. Electron Dev.* **67** 3898

[18] Wangsness R K 1979 *Electromagnetic fields* (New York: Wiley)

[19] Baliga B J 2010 *Fundamentals of power semiconductor devices* (Berlin: Springer Science & Business Media)

[20] Hou X Y, Huang R, Chen G, Liu S, Zhang X, Yu B and Wang Y Y 2008 *Chin. Phys. B* **17** 0685

[21] Chen S Z and Sheng K 2014 *Chin. Phys. B* **23** 077201

[22] Zhang W, Zhang B, Qiao M, Li Z, Luo X and Li Z 2016 *Trans. Electron Dev.* **63** 1984